J. Min. Metall. Sect. B-Metall. 61 (2) (2025) 223 - 233

Journal of Mining and Metallurgy, Section B: Metallurgy

CONSTITUTIVE ANALYSIS OF Cu-DHP ALLOY DURING HOT COMPRESSION

A. Kalhor [a], K. Rodak [a], M. Maleki [b], M.J. Sohrabi [b], M. Mobasheri [b, c], H. Mirzadeh [b, *], M. Habibi Parsa [b]

[a] Silesian University of Technology, Faculty of Materials Engineering, Katowice, Poland
[b] University of Tehran, School of Metallurgy and Materials Engineering, College of Engineering, Tehran, Iran
[c] EPFL, Laboratory of Construction Materials, Lausanne, Switzerland

(Received 31 December 2024; Accepted 02 September 2025)

Abstract

The hot deformation behavior of deoxidized high-phosphorus copper (Cu-DHP) was investigated during compressive deformation over a wide deformation temperature range of 200 to 1000 °C and strain rates ranging from 0.0005 to 0.4 s^{-1}. The flow curves related to the hot working regime (500 to 1000 °C) generally showed distinct peak stresses followed by a drop in flow stress after the peak point, revealing the occurrence of dynamic recrystallization (DRX). By increasing the Zener-Hollomon parameter, the cyclic flow curves were replaced by the single-peak ones and eventually to the characteristic dynamic recovery (DRV) curves. At temperatures below half the melting point, only DRV-type curves were observed. Constitutive analysis yielded an apparent activation energy of 274.1 kJ/mol, a hyperbolic sine power of 4.88, and a power law stress exponent of 5.27, resulting in flow stress equations describing material flow in the hot working regime. Moreover, the power law breakdown and the importance of deformation temperature during thermomechanical processing were also critically discussed based on the mathematical fitting, strain rate sensitivity index, and microstructural analysis for investigating grain refinement by DRX. Furthermore, a strain-compensated Arrhenius model was developed for prediction of flow curves, considering the initial flow hardening and the subsequent flow softening by DRX. These findings offer practical guidance for optimizing hot working conditions of Cu-DHP alloy, with deformation at high Zener-Hollomon parameters enabling full DRX and finer grain structures for improved performance.

Keywords: *Cu-DHP alloy; Hot deformation; Constitutive modeling; Power law breakdown; Strain rate sensitivity index*

1. Introduction

Copper alloys have widely been used in a variety of industries for over a century owing to their exceptional electrical and thermal conductivities [1–4]. Depending on the specific industry requirements, a wide range of copper alloys, such as brass, bronze, phosphor bronze, beryllium copper, etc., are available to meet the demands of various applications [5, 6]. Additionally, a range of high-purity copper grades, e.g., oxygen-free high-conductivity (OFHC) copper, electrolytic tough-pitch (ETP) copper, and deoxidized high-phosphorus copper (Cu-DHP), have been developed and extensively used [7, 8]. In order to comprehend material plasticity, optimize manufacturing processes, fine-tune mechanical properties, develop innovative alloys, and ensure product reliability, it is imperative to investigate both the hot deformation behavior and the constitutive relations that describe the material flow [9–11].

Accurate modeling of hot flow stress is vital in metal-forming processes, as effective mathematical simulations rely on a thorough understanding of the material flow dynamics [12–14]. In this context, widely used constitutive equations for hot working are represented by the power law and exponential law. Among these, the hyperbolic sine law describes flow stress as related to the Zener-Hollomon parameter $Z = \dot{\varepsilon} \exp(Q / RT)$, where Q denotes the deformation activation energy, $\dot{\varepsilon}$ is the strain rate, T refers to the absolute temperature, and R is the universal gas constant [15–17]. Nonetheless, a reliable constitutive equation to characterize hot deformation behavior will emerge from a thorough consideration of the effects of deformation conditions and material parameters.

The hot deformation and dynamic recrystallization (DRX) behavior of high-purity copper grades have also been investigated [18–24]. For example, Prasad and Rao [19] studied the hot deformation behavior of OFHC copper through hot compression tests conducted over a temperature range of 300–950 °C and strain rates between 0.001 and 100 s^{-1}. They characterized the DRX domains and found that the average grain size varies linearly with the Z

Corresponding author: hmirzadeh@ut.ac.ir

https://doi.org/10.2298/JMMB241231018K

parameter. The power law was used to derive the constitutive equation, resulting in a stress exponent of 5.18. In another study, Liu *et al.* [20] investigated the deformation behavior of T2 copper through hot compression tests in the temperature range of 20–800 °C and strain rates of 0.01–10 s^{-1} and reported that dynamic recovery (DRV) occurred between 20 and 450 °C, and DRX took place within the 500–800 °C temperature range. These authors also developed strain-compensated equations to describe flow stress based on the hyperbolic sine equation. Yang and Kim [21] reported that the stress exponent in the power law equation gradually increased by decreasing temperature, and they characterized the power law breakdown (PLB) regime. Mirzadeh [22] also proposed a physically based constitutive equation for the OFHC copper via consideration of the deformation mechanisms. Huang *et al.* [23] developed a flow stress prediction model based on machine learning methods, which is instrumental for the guidance of hot working of pure copper. Chen *et al.* [24] also developed a dislocation density-based constitutive model for the T2 copper during isothermal and time-variant deformation, which can precisely describe the flow behavior over a wide range of deformation conditions.

Despite systematic reports on high-purity copper grades, the hot deformation behavior and constitutive analysis of the Cu-DHP alloy, a widely used commercial alloy, remain largely unexplored. There are a few reports on friction stir processing [25] and friction stir welding [26] of Cu-DHP alloy, depicting the occurrence of DRX due to the increased temperature during friction stirring and applying severe plastic deformation (SPD). Iordache *et al.* [27] performed tensile tests on Cu-DHP samples at temperatures of 22 and 500 °C for speeds of 3 and 30 mm/min and also developed the Johnson-Cook model for the description of flow stress. Recently, Kalhor et al. [28] investigated the influence of sulfur content on the hot deformation behavior of Cu-DHP alloy at a narrow temperature range of 500 to 1000 °C, while Maleki et al. [29] developed processing maps for this temperature range. However, the hot deformation behavior of the Cu-DHP alloy over a wide temperature range, from low to high, remains to be investigated, which would provide a more complete understanding of Cu-DHP behavior. Moreover, a systematic investigation for the development of constitutive equations that consider PLB in the power law analysis, as well as to develop viable constitutive equations supported by microstructural observations. Furthermore, developing a strain-compensated Arrhenius model for predicting flow curves, which considers the initial flow hardening and the subsequent flow softening by DRX, would be quite useful. Therefore, the hot deformation behavior of this alloy at different deformation conditions and the constitutive equations should be developed. The present study is focused on addressing these subjects by providing a comprehensive analysis of the hot deformation behavior of Cu-DHP alloy over a wide temperature range, offering new perspectives and critical data not previously available for this industrial-grade alloy.

2. Experimental details

The as-received material was an as-cast Cu-DHP alloy with an average grain size of ~500 μm. The maximum impurity contents (in ppm) in the Cu-DHP copper (Cu: 99.96%) used in this work were as follows: P: 301, Zn: 5, Sn: 10, Fe: 10, Pb: 1, S: 4, Ni: 1, Mg: 2, and Si: 3. The specimens for the hot compression test were prepared according to the ASTM E209, with a height of 12 mm and a diameter of 8 mm. The hot compression tests were performed using a Zwick/Roell Z250 universal testing machine, with mica sheets used as lubricant to reduce barreling. Specimens were heated to the desired deformation temperature and held for 20 min to eliminate thermal gradients. The deformation temperatures ranged from 200 to 1000 °C and strain rates ranged from 0.0005 to 0.4 $s^{-1.}$ Samples were deformed up to a true strain of 0.8, which was followed by water quenching to preserve the deformed microstructure. Each compression test was repeated three times per sample to ensure the reproducibility of the results. After etching with a solution containing ethanol, hydrochloric acid, and ferric chloride, the selected microstructures were observed using an Olympus Vanox optical microscope. The average grain size was measured using the standard intercept method.

3. Results and discussion

3.1. Flow behavior

The obtained hot deformation flow curves are depicted in Figure 1. It can be seen that the flow stress generally increases with increasing strain rate at each deformation temperature. Moreover, a decrease in the deformation temperature leads to the increment of flow stress at a given strain rate. This can collectively be characterized based on the Z parameter. By increasing the Z values, the flow stress increases. Interestingly, the dependence of flow stress on the strain rate significantly depends on the deformation temperature, with this dependence increasing as temperature rises. A more detailed discussion of this relationship will be provided in a later section.

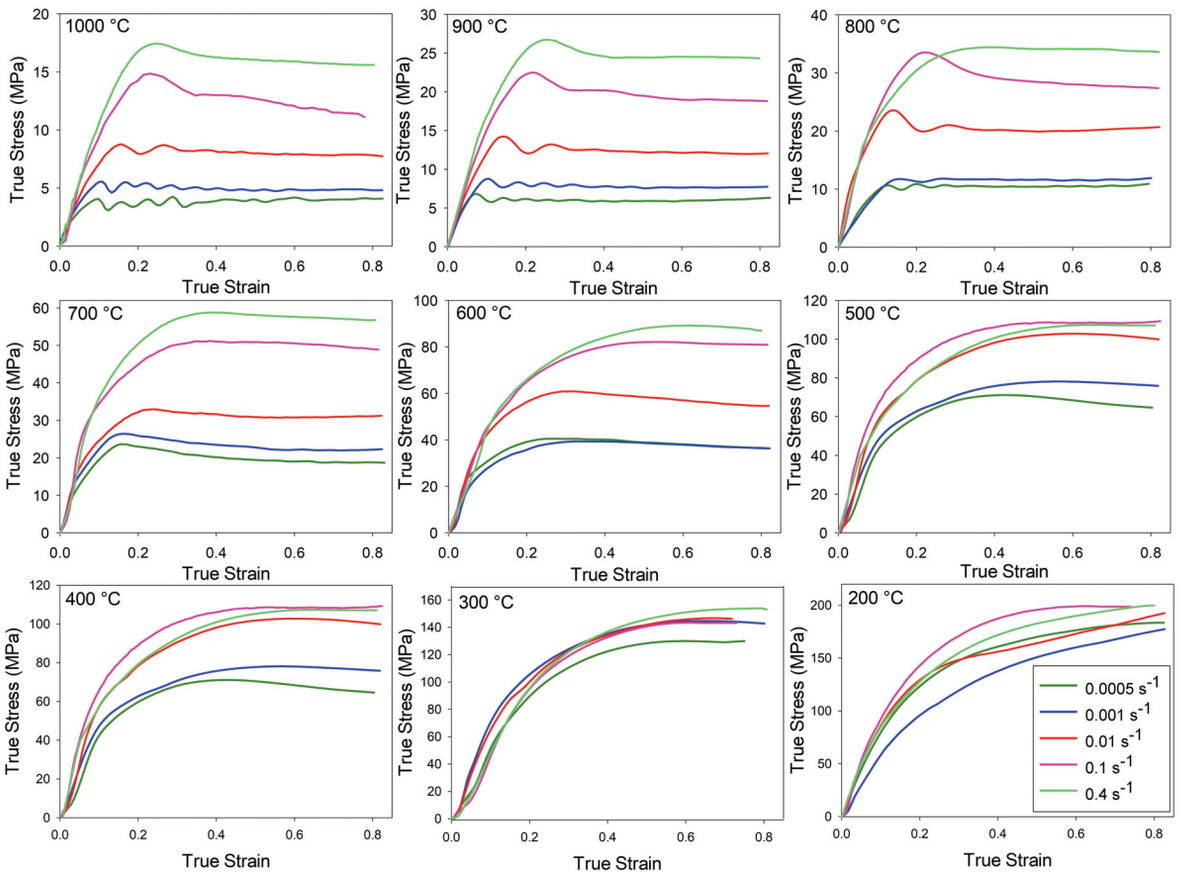

Figure 1. *Hot compression flow curves of the alloy at different temperatures and strain rates*

On the other hand, it is observable that the deformation temperature is quite important in the occurrence of the restoration mechanisms, resulting in the various characteristic flow behaviors. For instance, as can be seen for the deformation temperature of 1000 °C, all of the stress-strain curves depict the characteristic forms of the DRX flow curves, namely the single-peak and cyclic behaviors. By decreasing the strain rate (or decreasing the Z value), the single-peak flow curves are replaced by the cyclic ones. By decreasing the deformation temperature, the cyclic behavior tends to vanish, and the decrease of flow stress after the peak point becomes less pronounced. This can be related to the increased dislocation density in the newly formed DRX grains due to the decreased temperature, which leads to a less pronounced typical drop in flow stress after the peak point. It is noteworthy to mention that at high Z values, the peak stress might not appear at low strains, and hence, it needs higher strains [14, 30, 31]. At temperatures below 400 °C, typical DRV flow curves can be seen. The melting temperature (T_m) of pure Cu, as well as Cu-DHP [32], is 1356 K (1083 °C). Accordingly, $0.5T_m$ is 678 K (405 °C), which can be considered the lower boundary of the hot deformation range. Therefore, it is reasonable that the DRX does not occur at temperatures below 400 °C. As shown in this section, the considered ranges of deformation temperature and strain rate are broad enough to observe various flow behaviors.

3.2. Parameters of constitutive equations

For the hot deformation constitutive analysis, temperatures from 500 to 1000 °C were considered, which fall within the hot working range. The description of flow stress based on the temperature and strain rate necessitates specifying a characteristic strain. Hence, it is recommended to utilize characteristic stresses like steady-state and peak stresses, which represent the same deformation or softening mechanism in all flow curves. Typically, the peak stress (σ_p) is the most commonly used one for determining the hot working parameters, as it can be readily obtained by hot compression testing.

As demonstrated in Equation 1, the peak flow stress can be associated with Z using different basic

functions. The power law is preferred for describing flow behavior at lower stress levels. In contrast, the exponential law is applicable for relatively higher stresses in the PLB regime. Nonetheless, the hyperbolic sine law is applicable across a broad spectrum of temperatures and strain rates [33–36]:

$$Z = \dot{\varepsilon}\exp(\frac{Q}{RT}) = \begin{cases} A'\sigma_P^{n'} \Leftrightarrow \text{Power Law} \\ A''\exp(\beta\sigma_P) \Leftrightarrow \text{Exponential Law} \\ A\{\sin h(\alpha\sigma_P)\}^n \Leftrightarrow \text{Hyperbolic Sine Law} \end{cases} \quad (1)$$

where A, A', A'', n, n', β, and α ($\approx\beta/n'$) are the material constants. The stress multiplier α brings $\alpha\sigma_P$ into the correct range to make constant temperature curves in $ln\dot{\varepsilon}$ versus $\ln\{\sin h(\alpha\sigma_P)\}$ plots linear and parallel. Taking the natural logarithm from Equation 1 results in Equation 2:

$$\ln Z = \ln\dot{\varepsilon} + \frac{Q}{R}\times\frac{1}{T} = \begin{cases} \ln A' + n'\ln\sigma_P \\ \ln A'' + \beta\sigma_P \\ \ln A + n\ln\{\sin h(\alpha\sigma_P)\} \end{cases} \quad (2)$$

Based on Equation 2, the slopes of the $\ln\dot{\varepsilon} - \ln\sigma_P$ and $\ln\dot{\varepsilon} - \sigma_P$ plots at each temperature give the values of n' and β, respectively. The corresponding plots are depicted in Figures 2a and 2b. The average values of n' and β were determined as 8.3 and 0.252, respectively. Since α can be estimated as β/n' [37–40], the value of $\alpha \approx 0.03$ MPa^{-1} was obtained for the hot compression of Cu-DHP alloy.

Another application of Equation 2 is obtaining the average value of n based on the slopes of the $\ln\dot{\varepsilon} - \ln\{\sin h(\alpha\sigma_P)\}$ plots at each temperature. The required plots are shown in Figure 2c, leading to the value of n = 4.93 on average. Additionally, the hyperbolic sine description in Equation 2 can also be used to obtain the value of Q. This equation can be rewritten as follows:

$$\ln\{\sin h(\alpha\sigma_P)\} = \frac{-\ln A}{n} + \frac{\ln\dot{\varepsilon}}{n} + Q\cdot\frac{1}{RnT} \quad (3)$$

Accordingly, the slopes of the $\ln\{\sin h(\alpha\sigma_P)\} - 1/RnT$ plots at each strain rate give the values of Q, as shown in Figure 2d. As a result, the average value of Q was determined as 274.1 kJ/mol, which is close to the reported value of 261 kJ/mol for the OFHC copper by Blaz *et al.* [41].

Based on the obtained value of $\alpha \approx 0.03$ MPa^{-1} and Q = 274.1 kJ/mol, the constitutive analysis can be applied to all of the data points without the necessity of separate analysis at constant temperature or strain rate. Accordingly, the appropriate values of parameters such as n' and n can be obtained, which will be dealt with in the next section.

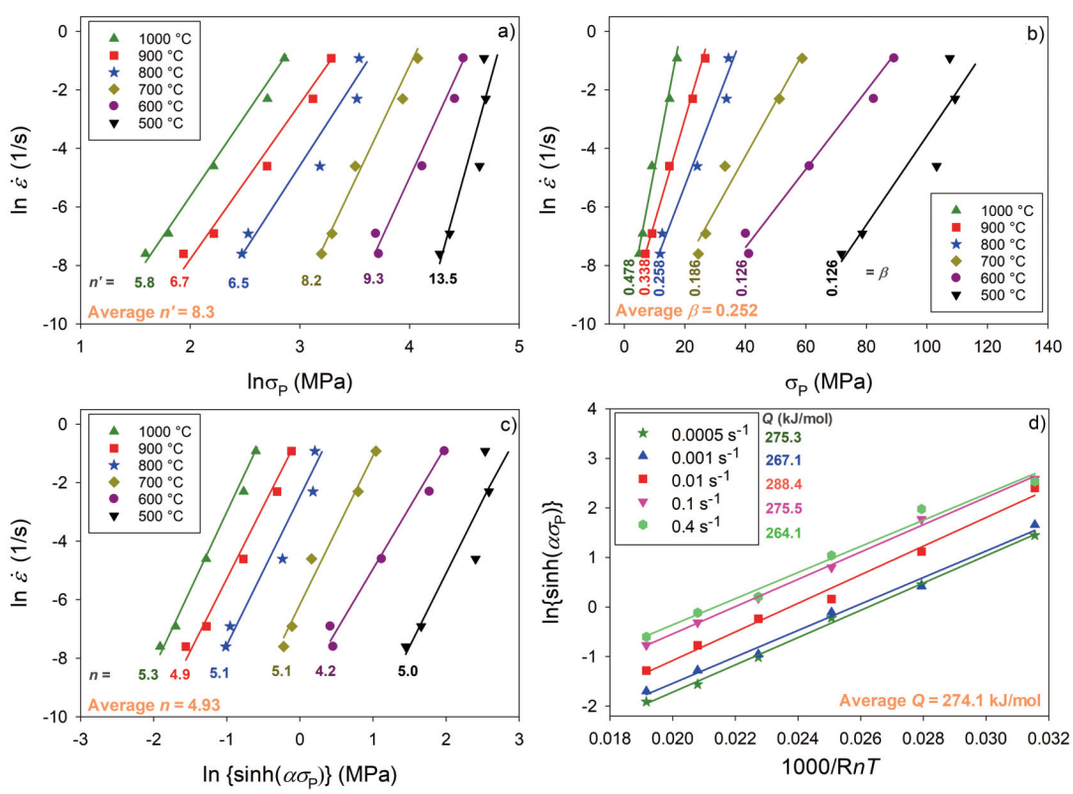

Figure 2. *Plots used for obtaining the parameters of constitutive equations: (a) n', (b) β, (c) n, and (d) Q*

3.3. Description of peak flow stress

By considering $\alpha \approx 0.03$ MPa^{-1} and $Q = 274.1$ kJ/mol in the hyperbolic sine description of flow stress in Equation 2, the slope and the intercept of the $\ln Z - \ln\{\sin h(\alpha\sigma_p)\}$ plot give the final values of n and $\ln A$, respectively. This plot is depicted in Figure 3a. As mentioned before, all of the flow data related to the hot deformation temperature range (500 to 1000 °C) were considered for this analysis. It can be seen that the fitted straight line is perfectly consistent with the data points, resulting in the following constitutive equation for the description of flow stress during hot compression of the Cu-DHP alloy:

$$Z = \dot{\varepsilon}\exp(\frac{274100}{RT}) = 1.12\times10^{12}\{\sin h(0.03\times\sigma_p)\}^{4.88} \quad (4)$$

In Figure 3a, the data points related to lower temperatures (200, 300, and 400 °C) are also shown. It can be seen that the deformation temperature of 400 °C, which is very close to the $T/T_m = 0.5$, also follows the fitted line. However, the data points related to low temperatures of 200 and 300 °C are located above the fitted line. This means that the flow stress is lower than that calculated based on the Z parameter in Equation 4. This deviation will be addressed subsequently.

By considering the power description of flow stress in Equation 2, the slope and the intercept of the $\ln Z$–$\ln\sigma_p$ plot give the final values of n' and $\ln A'$, respectively. This plot is depicted in Figure 3b, resulting in the following constitutive equation:

$$Z = \dot{\varepsilon}\exp(\frac{274100}{RT}) = 17240.21\times\sigma_p^{5.27} \quad (5)$$

It can be seen that the final value of n' is 5.27, which is close to the theoretical value of 5 for the typical mechanism of climb and glide of dislocations in the climb-controlled regime [42–46]. This value also aligns with the value of 5.18 obtained for the OFHC copper [18]. It is noteworthy that the power law is applicable to low-stress values (low Z). Accordingly, as shown in Figure 3b, some data points at high Z values are not consistent with the line related to the power law and instead follow a different relationship. However, the hyperbolic sine law in Figure 3a was able to describe the flow stress at both low and high Z values in the hot deformation regime. As expected from the discussion of Figure 3a, the data points corresponding to low temperatures of 200 and 300 °C in Figure 3b do not follow the curve fitted to the high Z data.

Figure 3a shows that the developed hyperbolic sine equation (Equation 4) shows a good agreement with the experimental results in the hot working regime. Beyond visual examination, the performance

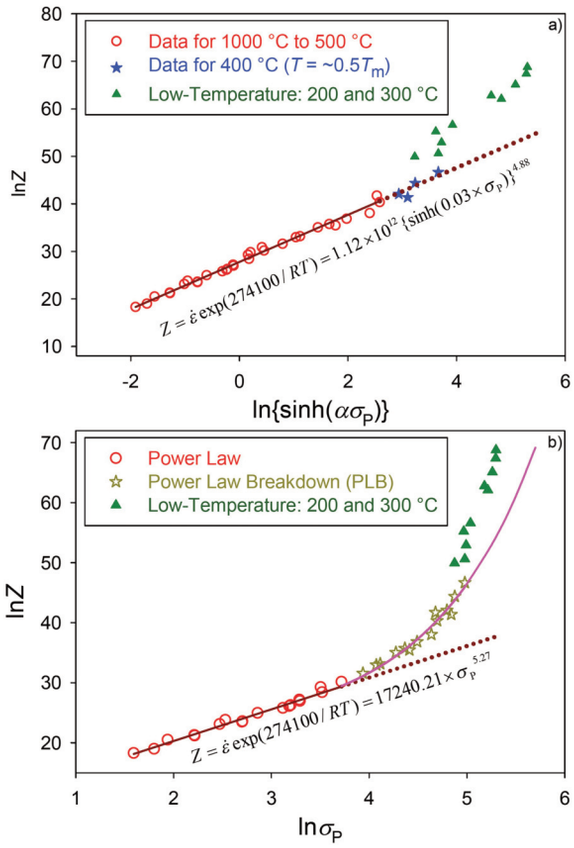

Figure 3. *Plots used for obtaining (a) n and lnA and (b) n' and lnA'*

of Equation 4 can be better evaluated by calculating the root mean square error (RMSE) and the average absolute relative error (AARE) using the following formulas [47, 48]:

$$RMSE = \sqrt{\frac{1}{N}\sum_{i=1}^{N}(t_i - y_i)^2} \quad (6)$$

$$AARE = \frac{1}{N}\sum_{i=1}^{N}\left|\frac{t_i - y_i}{t_i}\right|\times100 \quad (7)$$

where t_i is the target output, y_i is the model output, and N is the number of data points. The RMSE and AARE for the predictions of Equation 4 were determined as 3.64 MPa and 6.25%, respectively. These low error values confirm the applicability of Equation 4 in the prediction of peak flow stress.

3.4. Elucidating the effect of deformation temperature

As mentioned for Figure 1, the dependence of flow stress on the strain rate significantly depends on the deformation temperature, where this dependence increases with increasing temperature. To characterize

the effect of deformation temperature, the strain rate sensitivity index (m) was calculated at each temperature. According to $\sigma = C\dot{\varepsilon}^m$ and $Z = A'\sigma_P^{n'}$, the equation of $m = 1/n'$ can be derived. The results are depicted in Figure 4a. It can be seen that the m value generally increases with increasing temperature, where this increase becomes quite significant above 0.5 T_m. This is consistent with the general trend seen for various metals, where m rises rapidly with temperature at temperatures above $0.5T_m$ [49]. At elevated temperatures, atomic vibrations become significant, and each vibration can be considered a trial to overcome dislocation glide obstacles. The available number of trials directly depends on the available vibration time, which is determined by the strain rate [50]. This explains why strain rate becomes an important parameter at elevated temperatures. Therefore, a high dependence of flow stress on the strain rate is achieved, hence leading to an increased m value.

The next important observation in Figure 4a is the quite low m values at temperatures below $0.5T_m$ such as 200 and 300 °C. It is well-known that m is quite low near room temperature for most metals [49]. Accordingly, as mentioned earlier, the data points related to low temperatures of 200 and 300 °C are located above the fitted curves in Figures 3a and 3b. This means that the flow stress is lower than that calculated based on the Z parameter in Equation 4. This is related to the fact that at such low temperatures, the effect of strain rate becomes negligible due to m values near zero, negating the importance of the Z parameter.

To further demonstrate the effect of the deformation temperature, the optical micrographs of samples deformed at different temperatures at the lowest strain rate are depicted in Figures 4b to 4e. It can be seen that the microstructure deformed at 400 °C shows the large deformed as-cast grains, while at higher temperatures, fully recrystallized microstructures can be observed, revealing the operation of DRX at higher temperatures as the main restoration mechanism. These results are consistent with the observations made in Figure 4a, confirming that the deformation temperature of 400 °C or lower does not fall within the hot working regime. This observation also aligns with the report by Liu *et al.* [20] that showed that DRX occurred within the 500–800 °C temperature range in T2 pure copper. On the other hand, as shown in Figures 4c to 4e, increasing the deformation temperature significantly coarsens the DRX grain size due to the decrease in the Z value, as reported by several authors [18, 41, 51, 52]. Therefore, it is recommended to hot deform the Cu-DHP alloy at the highest Z value, which results in complete DRX with the finest grain size. It is noteworthy that the strain rate sensitivity analysis can be correlated with deformation and restoration mechanisms such as continuous DRX (CDRX) and/or discontinuous DRX (DDRX), which would provide greater scientific value. This important subject requires more in-depth microstructural analysis. It should also be mentioned that the presence of phosphorus in the Cu-DHP alloy might suppress grain coarsening during hot deformation and thermal processing. This effect may have contributed to the observed refinement of the DRX grains at high Z parameters.

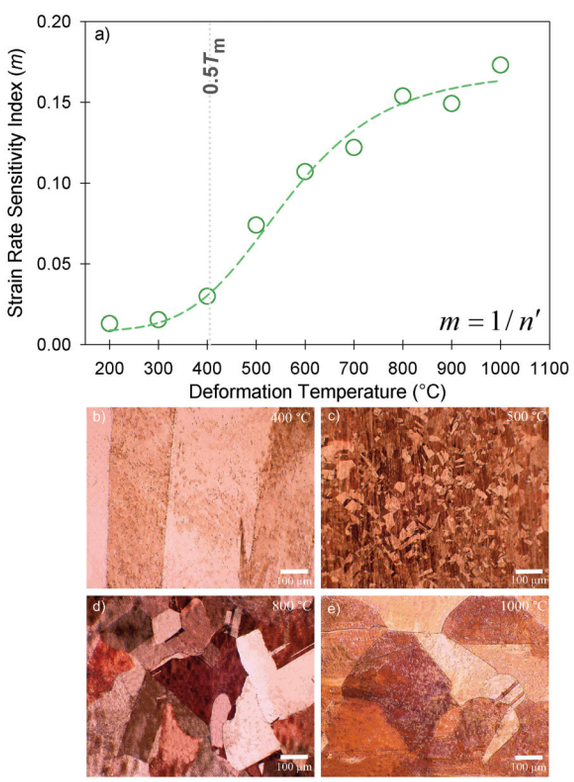

Figure 4. *(a) Dependency of m on the deformation temperature, and (b-e) microstructures of hot compressed samples deformed up to the true strain of 0.8 at different temperatures under a strain rate of 0.0005 s^{-1}*

3.5. *Modeling the flow curves*

The strain-compensated Arrhenius model was used to predict flow curves. In this technique, the procedure to obtain the values of A, n, α, and Q, as presented above, can be followed for a given strain. In this regard, instead of peak stress, the values of flow stress for a given strain at different deformation temperatures and strain rates can be used to calculate

the values of A, n, α, and Q for that strain. This process can be repeated for other strains, allowing the values of A, n, α, and Q to be correlated with strain [53–55]. Accordingly, in the present work, these calculations were performed for true strains from 0.1 to 0.8 at temperatures related to the hot working regime (500 to 1000 °C) and the results are summarized in Figure 5. It can be seen that A, n, α, and Q can be predicted by strain using the fitted equations shown in this figure. Therefore, upon calculating the values of A, n, α, and Q for each strain, the flow stress equation for that strain can be expressed as:

$$\sigma = \frac{1}{\alpha}\left\{\sin h^{-1}\left(\frac{Z}{A}\right)^{1/n}\right\} = \frac{1}{\alpha}\ln\left\{\left(\frac{Z}{A}\right)^{1/n} + \left\{\left(\frac{Z}{A}\right)^{2/n} + 1\right\}^{1/2}\right\} \quad (8)$$

Therefore, the flow stress at a given strain, deformation temperature, and strain rate can be calculated. Some examples are depicted in Figure 6, covering a wide range of flow stress levels. This model is capable of predicting the flow stress, and this technique can readily be used in future studies on the hot deformation of additively manufactured materials.

The RMSE and AARE for the strain-compensated Arrhenius model were determined as 3.72 MPa and 7.81%, respectively. These low error values confirm the applicability of the strain-compensated Arrhenius model for predicting flow stress.

Besides the models used in the present work, other viable approaches such as the mechanical threshold stress (MTS) theory [56–58], Zerilli-Armstrong (ZA) model [59], Johnson-Cook (JC) model [60], and artificial neural network (ANN) [61, 62] can also be used for modeling the flow stress. Regarding the ZA and JC models, the modified forms have successfully been used to consider the coupled effects of temperature, strain, and strain rate [63, 64]. These models can also be applied in future investigations on the hot deformation behavior of Cu-DHP alloy. This would provide better insight into flow stress modeling and accounts for both the flow hardening regime and flow softening by the DRX. Moreover, comparing different constitutive laws is quite useful when other models are considered. It should be noted that, while ANN and the other mentioned models could be applied, the strain-compensated Arrhenius model was chosen because it provides a physically meaningful description of hot deformation, directly linking flow stress to temperature, strain rate, and activation energy, while also capturing the effects of DRX.

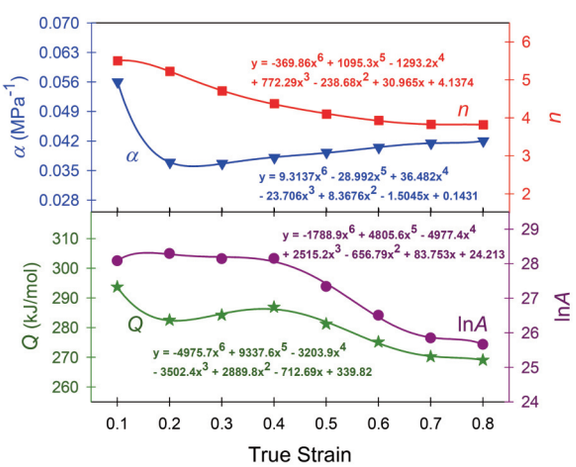

Figure 5. *Calculated values of α, n, lnA, and Q for different strains*

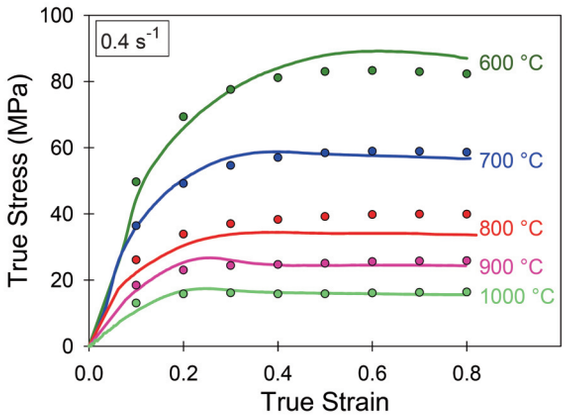

Figure 6. *Comparison of the calculated flow stress (circle points) with the original ones*

3.6. *Future prospects*

An interesting direction for future work is to use electron backscattered diffraction (EBSD) analysis to quantitatively investigate the DRX mechanisms, including the distinction between continuous and discontinuous DRX, to provide deeper insights into microstructural evolution. Furthermore, extending the study to higher strain rates (beyond 0.4 s^{-1}) could help improve understanding of the material's behavior under industrial conditions. These directions are promising and could broaden the applicability of the constitutive models developed in this work.

4. Conclusions

Constitutive behavior of the Cu-DHP alloy during hot compression testing was thoroughly investigated and critically analyzed. The key conclusions are as follows:

(1) The flow curves related to the hot working regime (500 to 1000 °C) generally showed distinct peak stresses, with flow stress decreasing after the peak point, revealing the occurrence of DRX. By

increasing *Z*, the cyclic flow curves were replaced by the single-peak curves and finally by the characteristic DRV curves. At temperatures below half of the melting point, only DRV-type curves were observed.

(2) Based on the constitutive analysis, the apparent activation energy of 274.1 kJ/mol, the hyperbolic sine power of 4.88, and the power law stress exponent of 5.27 were obtained, resulting in the following flow stress equations to describe material flow in the hot working regime:

$$Z = \dot{\varepsilon} \exp(\frac{274100}{RT}) = 1.12 \times 10^{12} \{\sin h(0.03 \times \sigma_P)\}^{4.88}$$

$$Z = \dot{\varepsilon} \exp(\frac{274100}{RT}) = 17240.21 \times \sigma_P^{5.27}$$

(3) The power law constitutive analysis identified three distinct deformation regimes: power law (low Z, larger DRX grains), power law breakdown (high Z, finer DRX grains), and low deformation temperature (no DRX). The strain rate sensitivity (*m*) increased significantly above $0.5T_m$, highlighting the critical role of deformation temperature. Practically, this defines an optimal hot working window above $0.5T_m$ (~400 °C) where fine, recrystallized grains form. Below this temperature, reduced DRX leads to coarser grains and higher flow stress.

(4) A strain-compensated Arrhenius model was developed to predict flow curves, considering the initial flow hardening and subsequent flow softening by DRX. The RMSE and AARE were determined to be 3.72 MPa and 7.81%, respectively, confirming the applicability of this model for predicting flow stress.

Authors contributions

Alireza Kalhor: Conceptualization, Formal analysis, Writing - Original Draft, Writing - Review & Editing. Kinga Rodak: Writing - Review & Editing. Milad Maleki: Methodology, Formal analysis, Investigation. Mohammad Javad Sohrabi: Conceptualization, Formal analysis, Writing - Original Draft, Writing - Review & Editing. Mohammad Mobasheri: Writing - Review & Editing. Hamed Mirzadeh: Conceptualization, Methodology, Visualization, Supervision, Writing - Review & Editing. Mohammad Habibi Parsa: Conceptualization, Supervision, Writing - Review & Editing.

Data availability

The authors stated that the processed data required to reproduce these findings were available in this manuscript.

Conflict of interest

The authors declare no conflict of interest.

Ethical statement

The manuscript has been prepared by the contribution of all authors, it is the original authors work, it has not been published before, it has been solely submitted to this journal, and if accepted, it will not be submitted to any other journal in any language.

Funding body

This work received no funding.

References

[1] D.F. Soares, M. Abreu, D. Barros, F. Castro, Experimental study of the Cu-Al-Sn phase equilibria, close to the copper zone, Journal of Mining and Metallurgy, Section B: Metallurgy, 53 (3) (2017) 209–213. https://doi.org/10.2298/JMMB170515034S

[2] Y. Liu, D. Liu, Y. Du, S. Liu, D. Kuang, P. Deng, J. Zhang, C. Du, Z. Zheng, X. He, Calculated interdiffusivities resulting from different fitting functions applied to measured concentration profiles in Cu-rich fcc Cu–Ni–Sn alloys at 1073 K, Journal of Mining and Metallurgy, Section B: Metallurgy, 53 (3) (2017) 255–262. https://doi.org/10.2298/JMMB170626022L

[3] Y. Ban, Y. Zhang, Y. Jia, B. Tian, A.A. Volinsky, X. Zhang, Q. Zhang, Y. Geng, Y. Liu, X. Li, Effects of Cr addition on the constitutive equation and precipitated phases of copper alloy during hot deformation, Materials & Design, 191 (2020) 108613. https://doi.org/10.1016/j.matdes.2020.108613

[4] A. Kalhor, K. Rodak, H. Myalska-Głowacka, B. Chmiela, K. Kuglarz, I. Schindler, K. Radwański, M. Kampik, High-strength and high-vonductivity Cu-0.7Mg-0.1Ca alloy fabricated via heat treatment and severe plastic deformation, Journal of Mining and Metallurgy, Section B: Metallurgy 61 (1) (2025) 43–58. https://doi.org/10.2298/JMMB241017004K

[5] I. Angela, I. Basori, B.T. Sofyan, Effect of cold rolling and annealing temperature to the characteristics of α+ β'phases in Cu-29.5 Zn-2.5 Al alloy produced by gravity casting, Journal of Mining and Metallurgy, Section B: Metallurgy, 56 (1) (2020) 89–97. https://doi.org/10.2298/JMMB180820037A

[6] S. Ghasemi, S. Vaghar, M. Pourzafar, H. Dehghani, A. Heidarpour, A novel predictive model for estimation of cell voltage in electrochemical recovery of copper from brass: application of gene expression programming, Journal of Mining and Metallurgy, Section B: Metallurgy, 56 (2) (2020) 237–245. https://doi.org/10.2298/JMMB190924012G

[7] E. Jiménez-Ruiz, R. Lostado-Lorza, C. Berlanga-Labari, A comprehensive review of fatigue strength in pure copper metals (DHP, OF, ETP), Metals, 14 (4) (2024) 464. https://doi.org/10.3390/met14040464

[8] S. Taylor, I. Masters, Z. Li, H.R. Kotadia, Direct observation via in situ heated stage ebsd analysis of

recrystallization of phosphorous deoxidised copper in unstrained and strained conditions, Metals and Materials International, 26 (2020) 1030–1035. https://doi.org/10.1007/s12540-019-00493-y

[9] D. He, X. Chen, Y.C. Lin, The improved physically-mechanism constitutive model for a Ni-Mo-Cr-based superalloy with the pre-precipitation of μ phase in hot forming, Journal of Alloys and Compounds, 997 (2024) 174934. https://doi.org/10.1016/j.jallcom.2024.174934

[10] K.A. Babu, S. Mandal, Regression based novel constitutive analyses to predict high temperature flow behavior in super austenitic stainless steel, Materials Science and Engineering: A, 703 (2017) 187–195. https://doi.org/10.1016/j.msea.2017.07.035

[11] S.A. Kareem, J.U. Anaele, O.F. Olanrewaju, E.D. Adewale, N.C. Osondu-Okoro, E.O. Aikulola, S.O. Falana, B. Gwalani, M.O. Bodunrin, K.K. Alaneme, Insights into hot deformation of medium entropy alloys: Softening mechanisms, microstructural evolution, and constitutive modelling—a comprehensive review, Journal of Materials Research and Technology, 29 (2024) 5369–5401. https://doi.org/10.1016/j.jmrt.2024.03.011

[12] P. Martin, J.A. Muñoz, B. Ferrari, A.J. Sanchez-Herencia, C. Aguilar, J.M. Cabrera, Microstructure and constitutive modeling of an ultrafine-grained refractory high-entropy alloy fabricated by powder metallurgy, Journal of Materials Research and Technology, 30 (2024) 7910–7926. https://doi.org/10.1016/j.jmrt.2024.05.166

[13] Y.C. Lin, J. Huang, H.-B. Li, D.-D. Chen, Phase transformation and constitutive models of a hot compressed TC18 titanium alloy in the α+β regime, Vacuum, 157 (2018) 83–91. https://doi.org/10.1016/j.vacuum.2018.08.020

[14] Z. Savaedi, R. Motallebi, H. Mirzadeh, A review of hot deformation behavior and constitutive models to predict flow stress of high-entropy alloys, Journal of Alloys and Compounds, 903 (2022) 163964. https://doi.org/10.1016/j.jallcom.2022.163964

[15] A. Belyakov, H. Miura, T. Sakai, Dynamic recrystallization under warm deformation of polycrystalline copper, ISIJ International, 38 (6) (1998) 595–601. https://doi.org/10.2355/isijinternational.38.595

[16] Y. Zhang, A.A. Volinsky, Q.-Q. Xu, Z. Chai, B. Tian, P. Liu, H.T. Tran, Deformation behavior and microstructure evolution of the Cu-2Ni-0.5Si-0.15Ag alloy during hot compression, Metallurgical and Materials Transactions A, 46 (2015) 5871–5876. https://doi.org/10.1007/s11661-015-3150-7

[17] K.K. Alaneme, S.A. Kareem, M.O. Bodunrin, Hyperbolic–sine constitutive model determined hot deformation mechanisms and workability response of Al–Zn/Cu and Al–Zn/SiC based composites, Results in Engineering, 19 (2023) 101255. https://doi.org/10.1016/j.rineng.2023.101255

[18] Y.V.R.K. Prasad, K.P. Rao, Kinetics and dynamics of hot deformation of OFHC copper in extended temperature and strain rate ranges, International Journal of Materials Research, 96 (2021) 71–77. https://doi.org/10.3139/ijmr-2005-0010

[19] Y.V.R.K. Prasad, K.P. Rao, Processing maps and rate controlling mechanisms of hot deformation of electrolytic tough pitch copper in the temperature range 300–950°C, Materials Science and Engineering: A, 391 (1–2) (2005) 141–150. https://doi.org/10.1016/j.msea.2004.08.049

[20] Y. Liu, W. Xiong, Q. Yang, J.-W. Zeng, W. Zhu, G. Sunkulp, Constitutive behavior and processing map of t2 pure copper deformed from 293 to 1073 K, Journal of Materials Engineering and Performance, 27 (2018) 1812–1824. https://doi.org/10.1007/s11665-018-3210-4

[21] J.Y. Yang, W.J. Kim, Examination of high-temperature mechanisms and behavior under compression and processing maps of pure copper, Journal of Materials Research and Technology, 9 (1) (2020) 960–968. https://doi.org/10.1016/j.jmrt.2019.11.036

[22] H. Mirzadeh, Physically based constitutive description of OFHC copper at hot working conditions, Kovove Materialy, 53 (2) (2015) 105–111. https://doi.org/10.4149/km_2015_2_105

[23] S.H. Huang, S.X. Chai, X.S. Xia, Q. Chen, D.Y. Shu, Compression deformation behavior and processing map of pure copper, Strength of Materials, 48 (2016) 98–106. https://doi.org/10.1007/s11223-016-9743-6

[24] G. Chen, Y. Jin, J. Wang, C. Zhang, Q. Chen, H. Zhang, X. Zhao, Z. Li, C. Xie, Z. Du, Dislocation density-based constitutive model and processing map for t2 copper during isothermal and time-variant deformation, Metals and Materials International, 28 (2022) 2134–2145. https://doi.org/10.1007/s12540-021-01109-0

[25] I. Galvao, A. Loureiro, D.M.E. Rodrigues, Influence of process parameters on the mechanical enhancement of copper-DHP by FSP, Advanced Materials Research, 445 (2012) 631–636. https://doi.org/10.4028/www.scientific.net/AMR.445.631

[26] R.M. Leal, C.M. Almeida Leitão, A. Loureiro, D.M.E. Rodrigues, P. Vilaça, Microstructure and hardness of friction stir welds in pure copper, Materials Science Forum, 636–637 (2010) 637–642. https://doi.org/10.4028/www.scientific.net/MSF.636-637.637

[27] D.M. Iordache, E.R. Oprescu, C.I. Malea, E.L. Nițu, M.O. Crăcănel, C. Bădulescu, Determination of Johnson-Cook material constants for copper using traction tests and inverse identification, IOP Conference Series: Materials Science and Engineering, 1182 (2021) 012032. https://doi.org/10.1088/1757-899X/1182/1/012032

[28] A. Kalhor, K. Rodak, M.J. Sohrabi, M. Maleki, M. Mobasheri, H. Mirzadeh, M. Habibi Parsa, Influence of sulphur content on the hot deformation behaviour and constitutive description of Cu-DHP alloy, Canadian Metallurgical Quarterly, (2025) 1–8. https://doi.org/10.1080/00084433.2025.2486614

[29] M. Maleki, M.J. Sohrabi, H. Farzad, H. Mirzadeh, M.H. Parsa, R. Miresmaeili, S.H. Razavi, Unraveling the effect of trace sulfur content on hot working behavior of Cu-DHP alloy: A study using processing maps, Materials Chemistry and Physics, 339 (2025) 130739. https://doi.org/10.1016/j.matchemphys.2025.130739

[30] M. Roostaei, M.H. Parsa, R. Mahmudi, H. Mirzadeh, Hot compression behavior of GZ31 magnesium alloy, Journal of Alloys and Compounds, 631 (2015) 1–6. https://doi.org/10.1016/j.jallcom.2014.11.188

[31] H. Mirzadeh, A. Najafizadeh, Extrapolation of flow curves at hot working conditions, Materials Science

and Engineering: A, 527 (7–8) (2010) 1856–1860. https://doi.org/10.1016/j.msea.2009.11.013

[32] A. Kumar, G.S. Brar, Numerical investigation of friction crush welding aluminium and copper sheet metals with flanged edges, in: E3S Web of Conferences, EDP Sciences, (2021) p. 1015.

[33] G. Zhao, Y. Tian, H. Li, L. Ma, Y. Li, J. Li, Microstructure evolution and dynamic recrystallization mechanisms of 316L stainless steel during hot deformation, Archives of Civil and Mechanical Engineering, 24 (2024) 35. https://doi.org/10.1007/s43452-023-00844-y

[34] C. Phaniraj, D. Samantaray, S. Mandal, A.K. Bhaduri, A new relationship between the stress multipliers of Garofalo equation for constitutive analysis of hot deformation in modified 9Cr–1Mo (P91) steel, Materials Science and Engineering: A, 528 (18) (2011) 6066–6071. https://doi.org/10.1016/j.msea.2011.04.025

[35] H. Mirzadeh, A comparative study on the hot flow stress of Mg–Al–Zn magnesium alloys using a simple physically-based approach, Journal of Magnesium and Alloys, 2 (3) (2014) 225–229. https://doi.org/10.1016/j.jma.2014.09.003

[36] H. Mirzadeh, Quantification of the strengthening effect of reinforcements during hot deformation of aluminum-based composites, Materials & Design 65 (2015) 80–82. https://doi.org/10.1016/j.matdes.2014.09.029

[37] H.J. McQueen, N.D. Ryan, Constitutive analysis in hot working, Materials Science and Engineering: A, 322 (1–2) (2002) 43–63. https://doi.org/10.1016/S0921-5093(01)01117-0

[38] R. Motallebi, Z. Savaedi, H. Mirzadeh, Additive manufacturing – A review of hot deformation behavior and constitutive modeling of flow stress, Current Opinion in Solid State and Materials Science, 26 (3) (2022) 100992. https://doi.org/10.1016/j.cossms.2022.100992

[39] H. Mirzadeh, Constitutive description of 7075 aluminum alloy during hot deformation by apparent and physically-based approaches, Journal of Materials Engineering and Performance, 24 (2015) 1095–1099. https://doi.org/10.1007/s11665-015-1389-1

[40] H. Mirzadeh, Quantification of the strengthening effect of rare earth elements during hot deformation of Mg-Gd-Y-Zr magnesium alloy, Journal of Materials Research and Technology, 5 (1) (2016) 1–4. https://doi.org/10.1016/j.jmrt.2015.03.001

[41] L. Blaz, T. Sakai, J.J. Jonas, Effect of initial grain size on dynamic recrystallization of copper, Metal Science, 17 (12) (1983) 609–616. https://doi.org/10.1179/030634583790420448

[42] T.G. Langdon, Identifying creep mechanisms in plastic flow, International Journal of Materials Research, 96 (2022) 522–531.

https://doi.org/10.3139/ijmr-2005-0096

[43] A.K. Mukherjee, An examination of the constitutive equation for elevated temperature plasticity, Materials Science and Engineering: A, 322 (1–2) (2002) 1–22. https://doi.org/10.1016/S0921-5093(01)01115-7

[44] H. Mirzadeh, J.M. Cabrera, A. Najafizadeh, Constitutive relationships for hot deformation of austenite, Acta Materialia, 59 (16) (2011) 6441–6448. https://doi.org/10.1016/j.actamat.2011.07.008

[45] H. Mirzadeh, Constitutive behaviors of magnesium and Mg–Zn–Zr alloy during hot deformation, Materials Chemistry and Physics, 152 (2015) 123–126. https://doi.org/10.1016/j.matchemphys.2014.12.023

[46] H. Mirzadeh, Simple physically-based constitutive equations for hot deformation of 2024 and 7075 aluminum alloys, Transactions of Nonferrous Metals Society of China, 25 (5) (2015) 1614–1618. https://doi.org/10.1016/S1003-6326(15)63765-7

[47] A. Rudra, S. Das, R. Dasgupta, Constitutive modeling for hot deformation behavior of Al-5083 + SiC composite, Journal of Materials Engineering and Performance, 28 (2019) 87–99. https://doi.org/10.1007/s11665-018-3813-9

[48] M. Alibeyki, H. Mirzadeh, M. Najafi, A. Kalhor, Modification of rule of mixtures for estimation of the mechanical properties of dual-phase steels, Journal of Materials Engineering and Performance, 26 (2017) 2683–2688. https://doi.org/10.1007/s11665-017-2687-6

[49] W.F. Hosford, Mechanical behavior of materials, Cambridge university press, 2010.

[50] J. Rösler, H. Harders, M. Bäker, Mechanical behaviour of engineering materials: metals, ceramics, polymers, and composites, Springer Science & Business Media, 2007.

[51] A. Belyakov, W. Gao, H. Miura, T. Sakai, Strain-induced grain evolution in polycrystalline copper during warm deformation, Metallurgical and Materials Transactions A, 29 (1998) 2957–2965. https://doi.org/10.1007/s11661-998-0203-1

[52] A.M. Wusatowska-Sarnek, The new grain formation during warm and hot deformation of copper, Journal of Engineering Materials and Technology 127 (3) (2005) 295–300. https://doi.org/10.1115/1.1925284

[53] Y.C. Lin, Y.-C. Xia, X.-M. Chen, M.-S. Chen, Constitutive descriptions for hot compressed 2124-T851 aluminum alloy over a wide range of temperature and strain rate, Computational Materials Science, 50 (1) (2010) 227–233. https://doi.org/10.1016/j.commatsci.2010.08.003

[54] D. Niu, C. Zhao, D. Li, Z. Wang, Z. Luo, W. Zhang, Constitutive modeling of the flow stress behavior for the hot deformation of Cu-15Ni-8Sn alloys, Frontiers in Materials, 7 (2020) 577867. https://doi.org/10.3389/fmats.2020.577867

[55] H.R. Rezaei Ashtiani, A.A. Shayanpoor, Prediction of thermo-mechanical behavior and microstructural evolution of copper considering initial grain size at elevated temperature, Materials Today Communications, 28 (2021) 102652. https://doi.org/10.1016/j.mtcomm.2021.102652

[56] L. Daridon, O. Oussouaddi, S. Ahzi, Influence of the material constitutive models on the adiabatic shear band spacing: MTS, power law and Johnson–Cook models, International Journal of Solids and Structures, 41 (11–12) (2004) 3109–3124. https://doi.org/10.1016/j.ijsolstr.2004.01.008

[57] L. Campagne, L. Daridon, S. Ahzi, A physically based model for dynamic failure in ductile metals, Mechanics of Materials, 37 (8) (2005) 869–886. https://doi.org/10.1016/j.mechmat.2004.06.006

[58] K. Le Mercier, J.D. Guérin, M. Dubar, L. Dubar, E.S. Puchi-Cabrera, Physically-based constitutive description of a commercial Al-Mg-Si alloy deformed under cold-warm working conditions, Journal of Alloys

and Compounds, 790 (2019) 1177–1191. https://doi.org/10.1016/j.jallcom.2019.03.113

[59] F.J. Zerilli, R.W. Armstrong, Dislocation-mechanics-based constitutive relations for material dynamics calculations, Journal of Applied Physics, 61 (1987) 1816–1825. https://doi.org/10.1063/1.338024

[60] G.R. Johnson, A constitutive model and data for metals subjected to large strains, high strain rates and high temperatures, in: Proceedings of the 7th International Symposium on Ballistics, The Hague, Netherlands, 1983.

[61] M.R. Zamani, H. Mirzadeh, M. Malekan, Artificial neural network applicability in studying hot deformation behaviour of high-entropy alloys, Materials Science and Technology, 39 (18) (2023) 3351–3359. https://doi.org/10.1080/02670836.2023.2231767

[62] M. Karimzadeh, M. Malekan, H. Mirzadeh, N. Saini, L. Li, Hot deformation behavior analysis of as-cast CoCrFeNi high entropy alloy using Arrhenius-type and artificial neural network models, Intermetallics, 168 (2024) 108240. https://doi.org/10.1016/j.intermet.2024.108240

[63] D. Samantaray, S. Mandal, U. Borah, A.K. Bhaduri, P. V Sivaprasad, A thermo-viscoplastic constitutive model to predict elevated-temperature flow behaviour in a titanium-modified austenitic stainless steel, Materials Science and Engineering: A, 526 (1–2) (2009) 1–6. https://doi.org/10.1016/j.msea.2009.08.009

[64] Y.C. Lin, X.-M. Chen, G. Liu, A modified Johnson–Cook model for tensile behaviors of typical high-strength alloy steel, Materials Science and Engineering: A, 527 (26) (2010) 6980–6986. https://doi.org/10.1016/j.msea.2010.07.061

KONSTITUTIVNA ANALIZA LEGURE Cu-DHP TOKOM TOPLE KOMPRESIJE

A. Kalhor [a], K. Rodak [a], M. Maleki [b], M.J. Sohrabi [b], M. Mobasheri [b, c], H. Mirzadeh [b, *], M.H. Parsa [b]

[a] Šlezijski tehnološki univerzitet, Fakultet za inženjerstvo materijala, Katovice, Poljska
[b] Univerzitet u Teheranu, Odsek za metalurgiju i inženjerstvo materijala, Tehnički fakultet, Teheran, Iran
[c] EPFL, Laboratorija za građevinske materijale, Lozana, Švajcarska

Apstrakt

Ponašanje tokom tople deformacije deoksidisanog bakra sa visokim sadržajem fosfora (Cu-DHP) je istraženo tokom kompresione deformacije u širokom opsegu temperatura deformacije od 200 do 1000 °C i brzina deformacije u rasponu od 0,0005 do 0,4 s^{-1}. Krive tečenja koje se odnose na režim tople obrade (od 500 do 1000 °C) generalno su pokazale izrazite vršne napone praćene padom napona tečenja nakon vršne tačke, otkrivajući pojavu dinamičke rekristalizacije (DRX). Povećanjem Zener-Holomonovog parametra, ciklične krive tečenja su zamenjene krivama sa jednim vrhom i na kraju karakterističnim krivama dinamičkog oporavka (DRV). Na temperaturama ispod polovine tačke topljenja, primećene su samo krive tipa DRV. Konstitutivna analiza je dala prividnu aktivacionu energiju od 274,1 kJ/mol, hiperbolički sinusni eksponent od 4,88 i eksponent napona zakona snage od 5,27, što je rezultiralo jednačinama napona tečenja koje opisuju protok materijala u režimu tople obrade. Štaviše, prekid zakona snage i važnost temperature deformacije tokom termomehaničke obrade su takođe kritički diskutovani na osnovu matematičkog prilagođavanja, indeksa osetljivosti na brzinu deformacije i mikrostrukturne analize za istraživanje usitnjavanja zrna pomoću DRX-a. Nadalje, razvijen je Arenijusov model kompenzovan deformacijom za predviđanje krivih tečenja, uzimajući u obzir početno očvršćavanje tokom tečenja i naknadno omekšavanje tečenjem pomoću DRX-a. Ovi nalazi nude praktične smernice za optimizaciju uslova tople obrade legure Cu-DHP, pri čemu deformacija pri visokim Zener-Holomonovim parametrima omogućava potpunu DRX i finije strukture zrna za poboljšane performanse.

Ključne reči: *Legura Cu-DHP; Topla deformacija; Konstitutivno modelovanje; Prekid zakona snage; Indeks osetljivosti na brzinu deformacije*